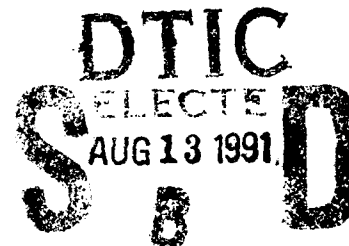AD-A239 502

Investigation of Interfacial Shear Strength in SiC/Si$_3$N$_4$ Composites

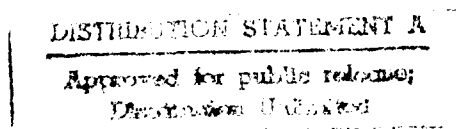J.I. Eldridge
Lewis Research Center
Cleveland, Ohio

R.T. Bhatt
Propulsion Directorate
U.S. Army Aviation Systems Command
Lewis Research Center
Cleveland, Ohio

and

J.D. Kiser
Lewis Research Center
Cleveland, Ohio

DTIC
ELECTE
AUG 13 1991
S B D

US ARMY
AVIATION
SYSTEMS COMMAND
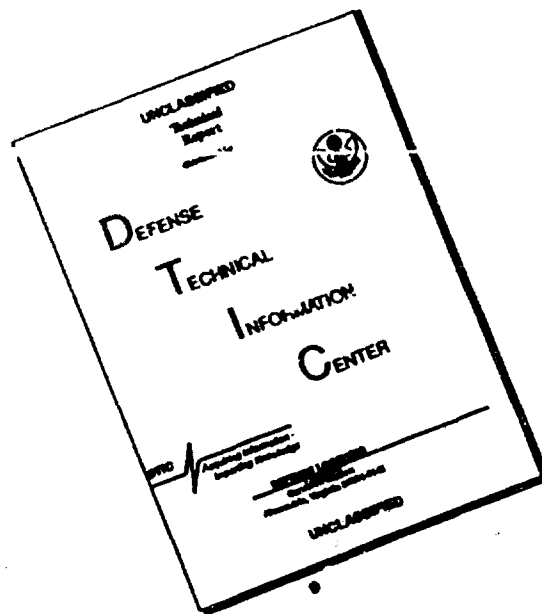AVIATION R&T ACTIVITY

NASA

91-07591

91 8 12 041

DISCLAIMER NOTICE

THIS DOCUMENT IS BEST QUALITY AVAILABLE. THE COPY FURNISHED TO DTIC CONTAINED A SIGNIFICANT NUMBER OF PAGES WHICH DO NOT REPRODUCE LEGIBLY.

INVESTIGATION OF INTERFACIAL SHEAR STRENGTH
IN SiC/Si$_3$N$_4$ COMPOSITES

J.I. Eldridge, R.T. Bhatt, and J.D. Kiser
National Aeronautics and Space Administration
Lewis Research Center
Cleveland, Ohio 44135

Summary

A fiber push-out technique was used to determine fiber/matrix interfacial shear strength (ISS) for silicon carbide fiber reinforced reaction-bonded silicon nitride (SiC/RBSN) composites in the as-fabricated condition and after consolidation by hot isostatic pressing (HIPing). In situ video microscopy and acoustic emission detection greatly aided the interpretation of push-out load/displacement curves. The as-fabricated and HIPed SiC/RBSN composites showed very different fiber push-out behavior as reflected by differently shaped load/displacement curves. The push-out data revealed the presence of definite, but weak, fiber/matrix bonding in both the as-fabricated composite and a composite HIPed at low temperature and showed the absence of fiber/matrix bonding in a composite HIPed at high temperature. The HIPed composites exhibited significantly higher frictional interfacial shear stresses as well as evidence of interfacial wear during fiber sliding. Finally, fiber push-out testing of different thickness samples revealed two regimes of fiber/matrix debonding behavior. For thinner samples, a single complete debonding event occurs; whereas, for thicker samples, a debond initiation of a critical length occurs and is followed by stable debond propagation with increasing applied load.

Introduction

Silicon carbide fiber reinforced reaction-bonded silicon nitride (SiC/RBSN) composite is a promising candidate material for component applications in advanced heat engines (ref. 1). Reinforcement of a RBSN matrix with SiC fibers has been shown to yield a material which shows greater strength and toughness (composite shows graceful failure beyond matrix cracking) than unreinforced RBSN of the same density. Results have shown that interfacial shear strength is one of the key properties that control the mechanical performance of the composite. If the interfacial shear strength is too high, the composite shows brittle behavior. If it is too low, however, the fiber/matrix load transfer is inadequate for optimum composite mechanical properties. Achieving optimum interfacial shear strength after fabrication and maintaining it during service is critical for composite performance. While most of the effort to improve composite properties has focused on improving matrix and fiber properties, it is important to determine how changes in composite processing affect the mechanical strength of the fiber/matrix interface. In the development of the SiC/RBSN composite, work is being done to increase the density of the RBSN matrix (ref. 2). In the as-fabricated state, the matrix has a porosity level of about 30 vol%. Hot isostatic pressing (HIPing) of SiC/RBSN containing a small concentration of MgO has been performed to fully densify the matrix, with the goal of increasing the oxidation resistance of the composite as well as increasing the matrix strength. It was not known how the HIPing process might change the properties of the fiber/matrix interface. Because it is difficult to deduce interfacial properties from bulk strength or toughness measurements, which depend on many factors, a fiber push-out test was chosen to test the interface more directly.

The objective of this study was to determine the influence of matrix densification by HIPing on the interfacial shear strength (ISS) of SiC/RBSN composites (both bonding and frictional components) by a fiber push-out test. Since being introduced by Marshall (ref. 3), fiber indentation has evolved into a popular technique for determining both frictional and bonding contributions to the fiber/matrix interfacial shear strength. Two basic methodologies with different equipment requirements and analysis have

developed, the choice of which is dictated by fiber diameter. For small diameter fibers (<30 μm), the thick-sample configuration originally used by Marshall (ref. 3) is usually followed. In this configuration, only a portion of the total fiber length experiences any sliding. For large diameter fibers (>100 μm), a thin-sample configuration, developed by Laughner et al. (refs. 4 and 5), is usually favored. In this configuration, the entire fiber length slides at a critical load.

Significant improvements in the fiber indentation techniques have recently been achieved. The foremost advance has been the continuous measurement of load and displacement during the test. This capability provides continuous monitoring of the progressive stages of fiber debond initiation, debond propagation, and fiber sliding. This has been achieved with an ultralow load indentation instrument (maximum applied load = 0.12 N) for small diameter fibers (refs. 6 and 7). For large diameter fibers, displacement control has been achieved using the crosshead motion of a universal testing machine (maximum load limited by strength of indenter)(ref. 8).

Another significant improvement in testing large diameter fibers has been accomplished by replacing the commonly used pointed pyramidal Vickers indenter with a flat-bottomed indenter. A flat-bottomed indenter applies the load more uniformly over the fiber end and allows higher load levels without fiber damage. While the first flat-bottomed indenters had tapered bodies (refs. 8 and 9), Eldridge and Brindley (ref. 10) used a nontapered cylindrical flat-bottomed punch which allows a much greater range of fiber displacement without the indenter contacting the matrix.

It has recently been shown that acoustic emission detection (refs. 10, 11 and 12) and video microscopy (ref. 10) can be used to help identify fiber debonding and sliding events. While earlier work at this laboratory (refs. 10 and 13) did not include generation of fiber push-out load/displacement curves, this paper will present data from an improved version of the testing apparatus in which load, acoustic emission, and video imaging of the test are all monitored simultaneously during crosshead-driven indenter displacements in a universal testing machine.

This paper will present fiber push-out load/displacement curves for both as-fabricated and HIPed SiC/RBSN composites. Acoustic emission and video microscopy are used to unambiguously identify features of the load/displacement curves. The location of interfacial failure and the extent of interfacial wear during fiber sliding, as revealed by SEM observation of pushed-out fibers, are shown to be reflected in the push-out load/displacement curves. Finally, the effect of interfacial roughness on fiber sliding behavior, an aspect often overlooked until recently (refs. 14 and 15), was examined by a fiber push-back test.

[1]Avco Specialty Materials, Textron, Inc., Lowell, MA.
[2]Union Carbide, New York, NY.

Experimental

Material

The starting materials for the SiC/RBSN composite fabrication were SCS-6 SiC monofilament[1] and high purity silicon powder[2] that had been attrition-milled to an average particle size of 0.3 μm. The SiC monofilament consists essentially of a 37 μm diameter pyrolytic graphite-coated carbon core surrounded by a SiC sheath with an outer diameter of 142 μm. The fiber has an approximately 3 μm thick coating consisting of SiC particles embedded in pyrolytic carbon. (ref. 16)

The composites were consolidated by conventional powder fabrication methods using fugitive polymer binder. A detailed description of the preform fabrication and nitridation schedule has been reported. (refs. 17 and 18) Briefly, the composites were fabricated by a three-step process. In the first step, SiC fiber mats and silicon cloths were pre-pared with fugitive polymer binders. The silicon cloths contained a small concentration of MgO. In the second step, alternate layers of SiC fiber mats and the silicon cloths were stacked in a metal die and pressed in a vacuum hot press at 1000 °C under an applied stress of 69 MPa for 1 hr. In the third step, SiC/Si preforms were heat-treated in high-purity (>99.999 percent) nitrogen at 1200 °C for 40 hr.

Some of the SiC/RBSN composite panels were further densified by HIPing encapsulated samples at two different temperatures under argon pressure. These composites are referred to as low and high temperature HIPed SiC/RBSN composites. The details of the HIPing procedure are described in reference 2. Typical dimensions of the as-fabricated and HIPed SiC/RBSN panels were 150 by 50 by 2.2 mm. Optical micrographs (fig. 1) of polished cross-sections of the as-fabricated and HIPed composites show the densification of the matrix due to HIPing.

For fiber push-out testing, samples of various thicknesses were sliced perpendicular to the fiber axes with a diamond saw, mechanically polished, and finally lapped on a 1 μm diamond lapping film.

Fiber Push-Out Test

A schematic of the fiber push-out apparatus is shown in figure 2. Specimens were mounted across several 750 μm wide channels machined into a support block, allowing fibers to be pushed out without resistance from the support block. The sample support block was secured to a two-axis translation table which allows positioning of individual fibers in the composite beneath the indenter. Alignment of indenter and fiber was assessed by observation through an optical microscope. Following the example of Bright et al. (ref. 8), an Instron load frame was used in a compression mode to drive the indenter at a constant speed of 50 μm/min.

This controlled displacement allowed acquisition of load/displacement curves. A 100 μm diameter, flat-bottomed tungsten carbide punch (ref. 10) was used as an indenter (fig. 3); the punch sustained loads up to about 40 N. This type of indenter provided near-uniform loading of the fiber and also allowed fiber displacements up to 1 mm without contact between the punch and the matrix. Load and acoustic emission (AE) data were collected at 50 msec intervals by a computer, and plots of load and AE versus crosshead displacement were generated. A unique feature of this test is the combination of in situ video imaging of both the top and bottom ends of the fiber during the push-out process with simultaneous AE detection. Video monitoring and recording was done in a split-screen format with simultaneous display of the load/displacement and AE/displacement curves as they were acquired, along with a TV image of the fiber being pushed out. This makes it possible to correlate features in the load/displacement curves with fiber debonding and sliding events.

Results

Fiber Push-out

Figures 4 to 6 show typical load versus crosshead displacement curves for various thicknesses of as-fabricated, high temperature HIPed, and low temperature HIPed SiC/RBSN. The shape of each load/displacement curve depends on the relative magnitudes of the debond and frictional ISS values, sample thickness, as well as whether interfacial damage or wear occurs during fiber sliding. From 10 to 30 fiber push-outs were performed for each specimen thickness.

Figure 4 shows the load/displacement curves for different thicknesses of as-fabricated SiC/RBSN composite. For the 2.31 mm thick sample (fig. 4(a)), there is an initial linear portion corresponding to the elastic response of the testing apparatus, followed by a sharp decrease in load at the moment of debonding. The peak load was identified as the debond load. Simultaneous with the sharp load decrease, there is a spike in the AE signal. After debonding, the load is solely due to frictional resistance. The frictional sliding load was taken to be the stable load which was attained after debonding. While figure 4(a) shows one complete interfacial debonding event, the load/displacement curves for thicker specimens (figs. 4(b) to (d)) are more complicated in that they show incremental or progressive debonding. Debond initiation occurs at the load (debond initiation load) where the load/displacement curve deviates from its initial slope. This was confirmed by the observation on the TV monitor of a small initial displacement of the top end of the fiber relative to the matrix without any movement of the bottom end. After initial debonding, the load/displacement curve continues with a lower slope until a sharp decrease in load occurs (the load drop becomes less pronounced for thicker samples),

corresponding to a final debonding event (final debond load). Simultaneous with this load decrease, initial movement of the bottom end of the fiber is observed, accompanied by an AE spike. In the region between the initial and final debonding, part of the interface remains bonded, while the rest of the interface experiences frictional sliding with resultant compression of the fiber. For the thicker samples, longer displacements after complete debonding were necessary before the load decreased to a nearly stable value. For this reason, the sliding friction load was arbitrarily taken to be the load obtained after a crosshead displacement of 35 μm past the debonding. The behavior is most complicated for the 7.37 mm sample (fig. 4(d)), where there was no typical post-debond behavior (sometimes there was a gradual decrease in load, and in other cases there was a continuous increase in load after debonding). The load/displacement curves for the as-fabricated SiC/RBSN composite are representative of composites where the debond ISS is significantly higher than the frictional ISS.

The fiber push-out results for the SiC/RBSN composite HIPed at high temperature (fig. 5) show no sharp load decrease or no AE spike to indicate debonding for the specimen thicknesses tested. For all thicknesses, the top of the fiber was observed to move during the initial portion of the load/displacement curve. Because the departure from linearity and initial fiber movement were so gradual, it was difficult to assign a debond load. Indeed, as will be shown later, the load/displacement curves could be fit well by a second order polynomial, with no linear portion, indicating a near-zero debond ISS. Simultaneous observation of both ends of the fibers during push-out testing revealed that while the top ends of the fibers moved at very low loads, the bottom ends of the fibers did not move until near the peak load. Thus, the peak value was assigned to be the frictional sliding load. The load/displacement curves for the SiC/RBSN composite HIPed at high temperature represent a case where frictional ISS is much greater than debond ISS.

The SiC/RBSN composite HIPed at low temperature (fig. 6) is also a case where the frictional ISS is much greater than the debond ISS, but where there is a more definite debond event. As with the as-fabricated composite, the load/displacement curves show a small, sharp decrease in load at the moment of debonding. After this decrease there is a slow continuous increase in load for tens of microns of fiber sliding. Observation of movement of both the top and bottom of the fiber confirmed that complete fiber sliding occurs immediately after debonding. Thus, the subsequent increase in load reflects an increase in frictional shear stress as the fiber is further displaced. This suggests a build-up of interfacial wear debris which would impede fiber sliding. Debond initiation loads for 2.26 (fig. 6(c)) and 2.95 mm slices were difficult to assign from the load/displacement curves, but were readily determined by the observed motion of the fiber ends. No AE was observed at debonding except for the 0.51 mm thick sample.

3

Figures 7 to 9 summarize the results of these push-out tests, for all three materials, as a function of sample thickness. From 10 to 30 push-outs were done for each specimen thickness. Initial and final debond loads as well as frictional sliding loads are plotted where appropriate. Figures 7(a) and 9 show that the initial debond load, $P_{initial\ debond}$, increases with sample thickness initially and then levels off. At the same time, $P_{final\ debond}$ increases roughly linearly with increasing sample thickness.

Calculations of τ_{debond} and $\tau_{friction}$ from push-out loads for these samples are complicated due to several thickness effects on the push-out loads. These effects include transition from complete to progressive debonding behavior, and nonuniform stresses at the interface, for example, due to Poisson expansion of the fiber under applied load. However, for thin samples, with single debonding events, these effects can be neglected, (refs. 10 and 13) and both the frictional and debond ISS values can be calculated by a simple equation which assumes the interfacial shear stress is uniform along the length of the fiber/matrix interface:

$$\tau = \frac{P}{2\pi R L_f} \tag{1}$$

where R is the fiber radius, L_f is the embedded fiber length (sample thickness), τ is the debond or frictional ISS, and P is the debond or frictional load.

The above treatment will only be valid up to a maximum sample thickness. This clearly does not hold for most of the sample thicknesses tested, except for $\tau_{friction}$ for the composite HIPed at high temperature, which shows linear behavior for all thicknesses tested (fig. 8). Thus, τ_{debond} and $\tau_{friction}$ calculations were based on data from the thinnest samples tested as they should come closest to following the linear behavior of equation 1. Estimates of τ_{debond} and $\tau_{friction}$ obtained in this manner are listed in table I.

Push-Out versus Push-In Measurements

The frictional ISS measurements were based on complete fiber sliding through thin samples (push-out or push-through). It is worthwhile to compare this approach (fig. 10(a)) to the other commonly used technique, push-in testing (fig. 10(b)), developed by Marshall (ref. 3), where a thick sample is used and only the top portion of the fiber moves. The push-in approach is usually followed for smaller diameter fibers (<30 μm). While equation 1 is used to calculate $\tau_{friction}$ values for complete fiber sliding, for the push-in measurement, $\tau_{friction}$ is calculated from the curvature of the load/displacement curve (no thickness dependence):

$$u = \frac{P^2}{4\pi^2 R^3 \tau_{friction} E_f} + \frac{P}{K_{machine}} \tag{2}$$

where u is the crosshead displacement, P is the applied load, R is the fiber radius, E_f is the fiber modulus, and $K_{machine}$ is the spring constant of the whole testing assembly. The

value of $\tau_{friction}$ can be calculated by fitting a second order polynomial to the crosshead displacement versus load data. Weihs and Nix (refs. 7, 19, and 20) showed that both approaches could be used for small diameter fibers (10 to 25 μm) if the sample was sufficiently thin to achieve complete fiber sliding before the maximum applied load was reached. Differences in $\tau_{friction}$ calculated from the two different methods were postulated to arise from artifacts due to sample bending. In the present study, a SiC/RBSN composite HIPed at high temperature was chosen to compare both approaches because this material showed no evident fiber/matrix bonding to complicate the analysis. A thickness of 1.93 mm was chosen as the thickest sample in which all fibers tested achieved complete fiber sliding before the maximum applied load was reached. Sample bending during push-out would be negligible for this thickness. Both approaches were applied to the same test data, and the results were compared. Figure 10(c) shows a fiber load/displacement curve for the 1.93 mm thick sample where, for about the first 25 μm of crosshead displacement, the opposite end of the fiber does not move. Equation 2 was used to fit to this portion of the curve and gave $\tau_{friction}$ = 27.9 MPa. The peak load was used to calculate ISS from equation 1 and gave $\tau_{friction}$ = 28.9 MPa. There is reasonable agreement between the two methods, although not always as close as this example. This agreement offers reassurance that both methods are determining the same quantity.

Push-Back Test

The effect of interfacial roughness on frictional shear stresses was examined by a fiber push-back test. As shown in figure 11 for an as-fabricated SiC/RBSN composite, after an initial push-out, the sample is flipped over, and the same fiber was pushed back. A pronounced valley in the load/displacement curve is observed as the fiber moves through its initial undisplaced position. This phenomenon has also been observed by Jero and Kerans (ref. 14). This decrease in load occurs because the undisplaced position is the only fiber position where the contacting fiber and matrix surfaces are in registry. The importance of interlocking rough surfaces to sliding friction was proposed by Morscher et al. (ref. 15) The clamping stress which the matrix exerts on the fiber increases as the fiber moves away from this interlocking position. The frictional shear stress is a product of the coefficient of sliding friction, μ, and the normal stress exerted on the fiber, σ_N:

$$\tau = \mu \sigma_N \tag{3}$$

The normal stress exerted on a displaced fiber will be greater than the stress exerted on an undisplaced fiber due to interfacial roughness; thus, the minimum load observed as the fiber slides through its initial undisplaced position may be a better indication of the normal stress exerted on the undisplaced fiber.

4

Figure 12 shows, for all three composites, combined push-out and push-back load/displacement curves where the initial fiber displacements were very small. For the as-fabricated sample (fig. 12(a)), the load decreases almost to zero at the minimum of the load valley; the load valleys for the HIPed samples are similar in amplitude but start from a higher value (figs. 12(b) and (c)). Figure 13 also shows combined push-out and push-back load/displacement curves with longer initial fiber displacements. Note that while the valley remains narrow for the as-fabricated SiC/RBSN, it is severely broadened for both HIPed samples when the initial displacement is increased.

Location of Interfacial Failure

SEM observation of pushed-out fibers revealed that the type of interfacial failure which occurred was quite different for each of the materials investigated. Figure 14(a) shows the C-rich double coating on an undisplaced SCS-6 fiber in an as-fabricated SiC/RBSN composite. Interfacial failure for the as-fabricated SiC/RBSN composite occurred between these two C-rich fiber coatings, with no obvious damage to the exposed surfaces (fig. 14(b)). In contrast, figures 14(c) and (d) show that failure occurred between the matrix and the outer C-rich coating for the SiC/RBSN composite HIPed at high temperature. Note that the surface of the fiber coating is very rough with many asperities (fig. 14(d)). Some longitudinal grooving of the surface of the pushed-out fiber was also observed. In addition to this grooving, the exposed fiber surface was observed to become smoother along the length of the pushed-out fiber, until, at sufficiently great distances from the fiber end (e.g., 100 μm), no asperities were visible. Interfacial failure for fibers pushed out of the SiC/RBSN composite HIPed at low temperature (figs. 14(e) and (f)) was more complicated in that failure occurred at both the inter-coating interface and the SiC-sheath/inner-coating interface. Because sliding often occurred at both interfaces on the same fiber, the inner coating would, in those cases, be displaced less than the SiC fiber sheath as seen in figures 14(e) and (f). In addition, the inner C-rich coating was in most cases damaged, as evidenced by cracks or missing sections.

Discussion

The fiber push-out tests revealed differences in the debonding and frictional behavior of the fiber/matrix interfaces in as-fabricated, low temperature HIPed, and high temperature HIPed SiC/RBSN composites containing a small concentration of MgO. The observed differences in fiber push-out behavior should not be interpreted as only due to differences in matrix density, as the HIPing process also changes the chemistry and roughness of the fiber/matrix interface region. Convoluted in these data are effects of

sample thickness and interfacial wear, which are also of practical importance.

For all three composites, the debond ISS was very low (see table I and figs. 7 to 9); indeed, too low to measure for the composite HIPed at high temperature. For the as-fabricated SiC/RBSN composite, a load of 4.0 N was required to produce the critical length debond of about 3 mm. For the composite HIPed at low temperature, a load of 6.5 N was required to produce the critical length debond of about 1.5 mm. This behavior is consistent with an initial debond or crack initiation of a critical length followed by a stable debond or crack propagation with increasing load.

The most striking difference in push-out behavior for the three composites was in the frictional resistance to fiber sliding. While the as-fabricated SiC/RBSN showed a very low $\tau_{friction}$ of 1 to 2.5 MPa, the HIPed samples showed much higher values (28 MPa for the SiC/RBSN HIPed at high temperature). The load/displacement curves also showed evidence of interfacial wear playing an important role in $\tau_{friction}$. The evidence for this is the strongest for the composite HIPed at low temperature (fig. 6), where the frictional resistance keeps increasing well after the point at which the whole fiber has started to move. This may be explained by a build-up of wear debris at the fiber/matrix interface which would increase resistance to fiber movement. In addition, the load minimum observed in the fiber push-backs (figs. 12 and 13) is severely broadened following longer initial forward displacements for the HIPed samples (figs. 13(b) and (c)), suggesting that the greater interfacial wear which would occur over the longer sliding length has made the "reseating" position less distinct. It should be noted that while the composite HIPed at high temperature shows a severely broadened load valley during push-backs from longer displacements (fig. 13(c)), it does not show increasing frictional resistance after complete fiber sliding begins (see fig. 5). On the contrary, the frictional resistance decreases much more rapidly than would be expected from a simple loss of interfacial contact area as the fiber is pushed out. A different type of wear behavior is occurring here, possibly the breaking off of asperities along the interface which would make it easier to continue displacing the fiber.

The location of interfacial failure should be considered in comparing the interfacial debonding and frictional sliding response of the three materials. It is proposed that the different interfacial failure locations as observed by SEM (fig. 14) affect the resistance to fiber sliding as follows. The clean failure between the two C-rich coatings in the as-fabricated composite (fig. 14(b)) results in negligible wear at the sliding interface and nearly reversible post-debond push-out behavior. This interface offers the easiest sliding path between two relatively smooth, compliant surfaces. The uneven failure and inner coating fracture which occur for the composite HIPed at low temperature (figs. 14(e) and (f)) lead to an accumulation of wear debris from the pieces of

5

fractured coating trapped between the matrix and the sliding fiber. This build-up leads to an increasing resistance to fiber sliding. The failure between the outer C-rich coating and the Si_3N_4 matrix in the composite HIPed at high temperature (figs. 14(c) and (d)) indicates an absence of large wear debris. However, the coating surface exposed from fiber push-out shows many small asperities. The small observed asperities (fig. 14(d)) are broken or worn away as the fiber moves, as confirmed by observation with SEM of the smoothing of the exposed coating surface over greater sliding distances. The breaking of these asperities may explain both the initially high frictional resistance and its relatively rapid decrease once the fiber starts to move.

There may be advantages for the low τ_{debond} and relatively high $\tau_{friction}$ values observed for the HIPed material. The low debond ISS may retain the crack deflection capability of the as-fabricated material, while the higher frictional resistance to fiber sliding provides better fiber/matrix load transfer after debonding, allowing the fibers to carry significant loads. In addition, the increasing friction observed for the composite HIPed at low temperature would make it increasingly difficult to continue opening up a matrix crack. Some minimal debond ISS may be needed (perhaps 10 MPa (ref. 21)), especially for transverse properties where interfacial friction does not provide any fiber/matrix load transfer. Thus, the higher debond ISS observed for the composite HIPed at low temperature may offer an advantage over the very low debond ISS observed for the composite HIPed at high temperature. Tensile tests of these materials will be needed to confirm these predictions.

Summary of Results

1. The as-fabricated and HIPed SiC/RBSN composites showed contrasting fiber push-out behavior as reflected by differently shaped load/displacement curves. The characteristic shapes of these curves revealed the presence of definite, but weak, fiber/matrix bonding in the as-fabricated composite and the composite HIPed at low temperature, and the absence of fiber/matrix bonding in the composite HIPed at high temperature. Also the HIPed composites showed significantly higher frictional resistance to fiber sliding.

2. Correlation of SEM observation of pushed-out fibers with push-out load/displacement curves suggests that the location and topography of the interface that fails is critical to fiber sliding behavior and may govern whether interfacial wear occurs during fiber sliding.

3. Interfacial debonding showed two regimes of sample thickness dependence (except for the high-temperature HIPed composite where no debonding events were detected). Below a critical sample thickness, a single debonding event occurs at a load which increases with increasing sample thickness. Above a critical sample thickness, debond initiation of a

critical length occurs at a load independent of sample thickness. The debond then propagates in a stable manner with increasing applied load.

4. Values of $\tau_{friction}$ determined from both fiber push-out (thin sample) and push-in (thick sample) tests were in good agreement in the simple case where there was no fiber/matrix bonding.

Conclusions

A fiber push-out test has been developed in which in situ video microscopy and acoustic emission detection aid in the identification of fiber debonding and sliding events in fiber push-out load/displacement curves. This technique showed that HIPing significantly affects the fiber debonding and sliding behavior. The effect of these changes on bulk mechanical properties needs to be determined. Any observed relationship between push-out behavior and bulk mechanical properties should be considered for interfacial design.

References

1. Bhatt, R.T.: The Properties of Silicon Carbide Fiber Reinforced Silicon Nitride Composites. Whisker- and Fiber-Toughened Ceramics, R.A. Bradley, et al., eds., ASM International, 1988, pp. 199-208.

2. Bhatt, R.T.; and Kiser, J.D.: Matrix Density Effects on the Mechanical Properties of SiC/RBSN Composites. NASA TM-103098, 1990.

3. Marshall, D.B.: An Indentation Method For Measuring Matrix-Fiber Frictional Stresses in Ceramic Composites. J. Am. Ceram. Soc., vol. 67, no. 12, Dec. 1984, pp. C258-C259.

4. Laughner, J.W., et al.: Simple Indentation Method for Measurement of Interfacial Shear Strength in SiC/Si$_3$N$_4$ Composites. Ceram. Eng. Sci. Proc., vol. 7, no. 7-8, July-Aug. 1986, p. 932.

5. Laughner, J.W.; and Bhatt, R.T.: Measurement of Interfacial Shear Strength in SiC-Fiber/Si$_3$N$_4$ Composites. J. Am. Ceram. Soc., vol. 72, no. 10, Oct. 1989, pp. 2017-2019.

6. Marshall, D.B.; and Oliver, W.C.: Measurement of Interfacial Mechanical Properties in Fiber-Reinforced Ceramic Composites. J. Am. Ceram. Soc., vol. 70, no. 8, Aug. 1987, pp. 542-548.

7. Weihs, T.P.; and Nix, W.D.: Direct Measurements of the Frictional Resistance to Sliding of a Fiber in a Brittle Matrix. Scripta Met., vol. 22, no. 2, Feb. 1988, pp. 271-275.

8. Bright, J.D., et al.: Interfacial Bonding and Friction in Silicon Carbide (Filament)-Reinforced Ceramic- and Glass-Matrix Composites. J. Am. Ceram. Soc., vol. 72, no. 10, Oct. 1989, pp. 1891-1898.

9. Brun, M.K.; and Singh, R.N.: Effect of Thermal Expansion Mismatch and Fiber Coating on the Fiber Matrix Interfacial Shear Stress in Ceramic Matrix Composites. Adv. Ceram. Mater., vol. 3, no. 5, 1988, pp. 506-509.

10. Eldridge, J.I.; and Brindley, P.K.: Investigation of Interfacial Shear Strength in a SiC Fibre/Ti-24Al-11Nb Composite by a Fibre Push-Out Technique. J. Mater. Sci. Lett., vol. 8, no. 12, Dec. 1989, pp. 1451-1454.

11. Rouby, D.; and Osmani, H.: Characterization of Interface Debonding in a Ceramic-Ceramic Fiber Composite Using the Indentation Method and Acoustic-Emission. J. Mater. Sci. Lett., vol. 7, no. 11, Nov. 1988, pp. 1154-1156.

6

12. Netravali, A.N., et al.: Continuous Micro-Indenter Push-Through Technique for Measuring Interfacial Shear Strength of Fiber Composites. Composites Sci. Technol., vol. 34, no. 4, 1989, pp. 289-303.

13. Eldridge, J.I.; and Honecy, F.S.: Characterization of Interfacial Failure in SiC Reinforced Si_xN_y Matrix Composite Material by both Fiber Push-Out Testing and Auger Electron Spectroscopy. J. Vac. Sci. Technol. A, vol. 8, no. 3, pt. 1, May-June 1990, pp. 2101-2106.

14. Jero, P.D.; and Kerans, R.J.: The Contribution of Interfacial Roughness to Sliding Friction of Ceramic Fibers in a Glass Matrix. Scripta Met. Mater., vol. 24, no. 12, Dec. 1990, pp. 2315-2318.

15. Morscher, G.; Pirouz, P.; and Heuer, A.H.: Temperature Dependence of Interfacial Shear Strength in SiC-Fiber-Reinforced Reaction-Bonded Silicon-Nitride. J. Am. Ceram. Soc., vol. 73, no. 3, Mar. 1990, pp. 713-720.

16. Pirouz, P.; Morscher, G.; and Chung, J.: Importance of Interfacial Strength on Fracture-Toughness of Brittle Matrix Composites. Surfaces and Interfaces of Ceramic Materials, L. Dufour, et al., eds., Kluwer Academic Publishers, 1989, pp. 737-760.

17. Bhatt, R.T.: Method of Preparing Fiber-Reinforced Ceramic Materials. U.S. Patent 4,689,188, 1987.

18. Bhatt, R.T.: Mechanical Properties of SiC Fiber-Reinforced Reaction-Bonded Si_3N_4 Composites. NASA TM-87085, 1985.

19. Weihs, T.P.; Dick, C.M.; and Nix, W.D.: The Frictional Resistance to Sliding of a SiC Fiber in a Brittle Matrix. High-Temperature/High-Performance Composites, MRS Symp. Proc. Vol. 120, F.D. Lemkey, et al., eds., Materials Research Society, Pittsburgh, PA, 1988, pp. 247-252.

20. Weihs, T.P.; and Nix, W. D.: Experimental Examination of the Push-Down Technique for Measuring the Sliding Resistance of Silicon Carbide Fibers in a Ceramic Matrix. J. Am. Ceram. Soc., vol. 74, no. 3, Mar. 1991, pp. 524-534.

21. Bhatt, R.T.: Influence of Interfacial Shear Strength on the Mechanical Properties of SiC Fiber Reinforced Reaction-Bonded Silicon Nitride Matrix Composites. NASA TM-102462, 1990.

TABLE I.—ESTIMATES OF DEBOND AND FRICTIONAL ISS[a]

Composite	τ_{debond}, MPa	$\tau_{friction}$, MPa
As-fabricated[b]	3.0 ± 0.5	1.05 ± 0.22
Low temp. HIPed[c]	13.1 ± 2.2	32.4 ± 6.2[d]
High temp. HIPed[e]	--------[f]	29.4 ± 6.9

[a] Using data from thinnest samples tested of as-fabricated and low T HIPed composite. All sample thicknesses were used for high T HIPed composite.

[b] Data are for 2.31 mm thick sample.

[c] Data from 0.51 mm thick sample.

[d] Corresponds to peak load which occurs well beyond point of complete fiber sliding.

[e] From least squares fit to data from all thicknesses where complete fiber sliding was attained.

[f] No debond detected.
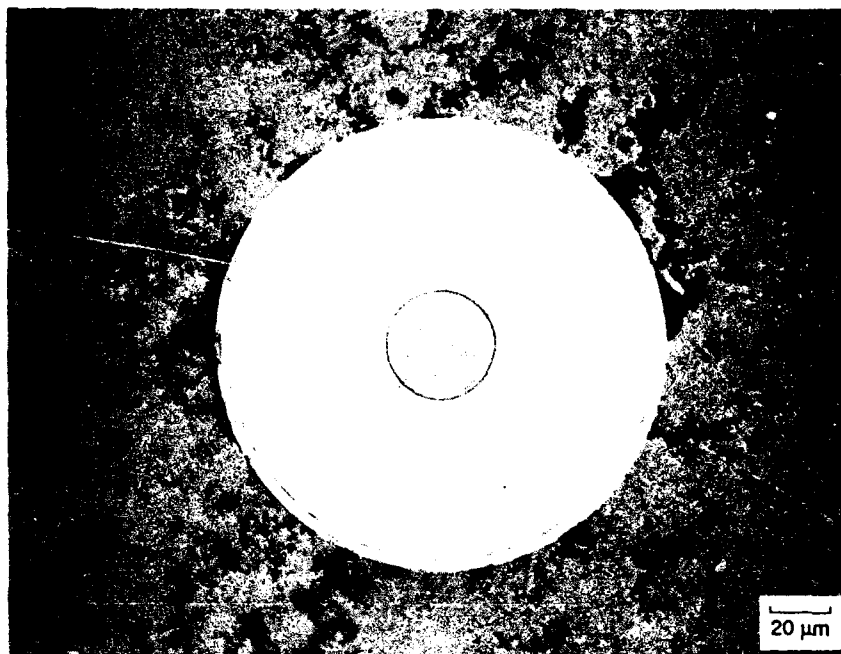
(a) As-fabricated.
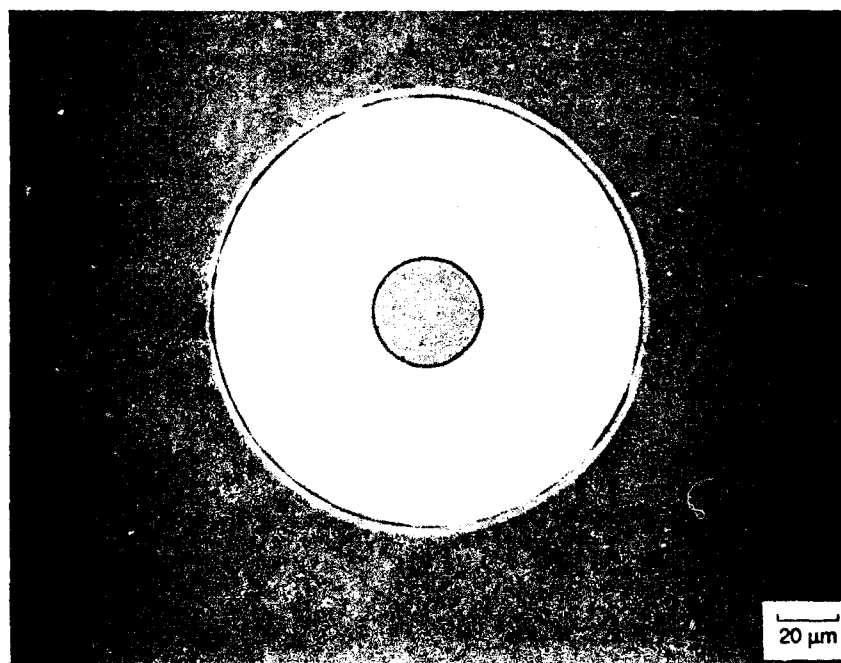
(b) HIPed at low temperature.

Figure 1.—Optical micrographs of SiC/RBSN composite containing MgO.
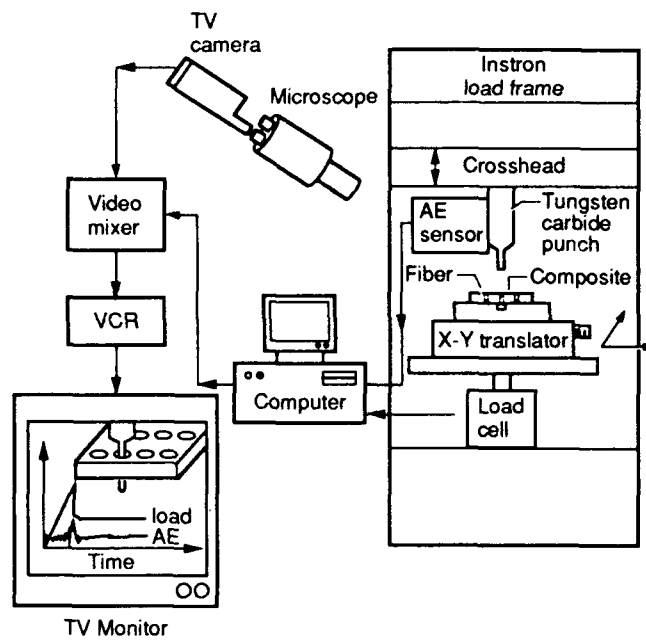
Figure 2.—Schematic representation of the fiber push-out apparatus.
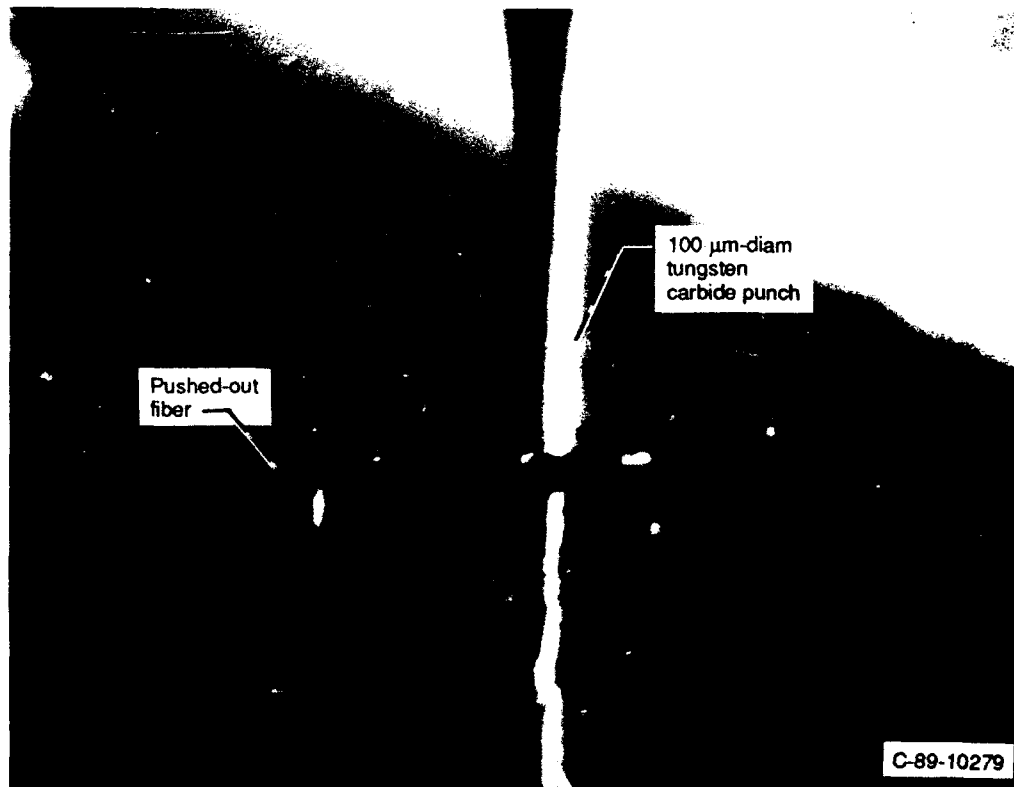
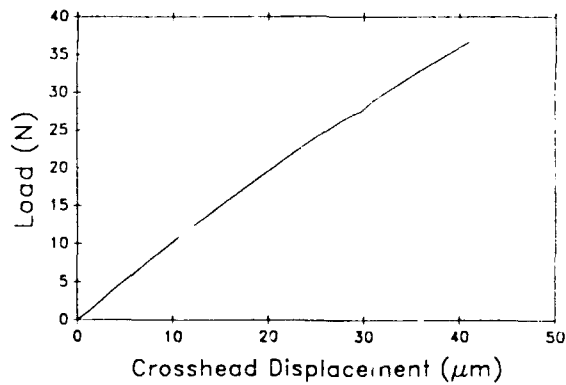Figure 3.—Optical micrograph of 100 μm diam tungsten carbide punch positioned above SCS-6 fiber in a SiC/RBSN composite.
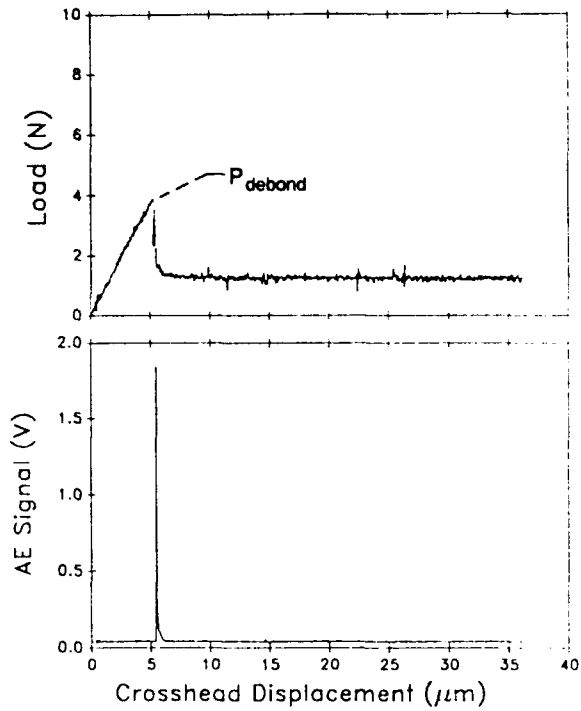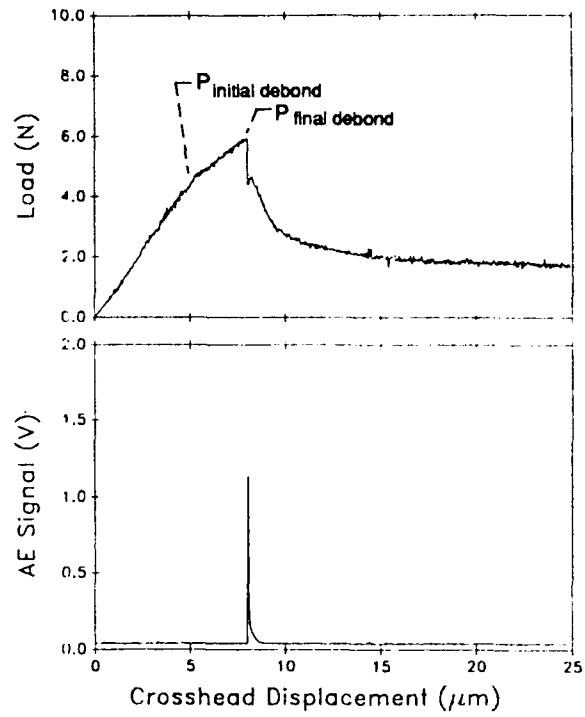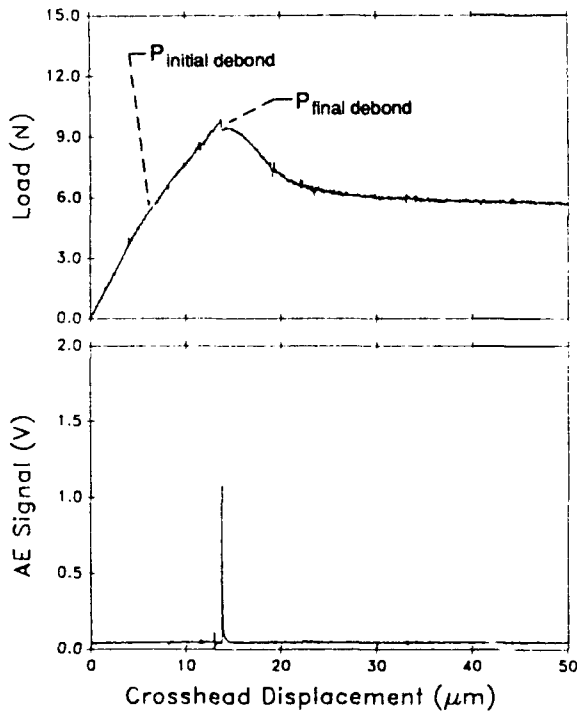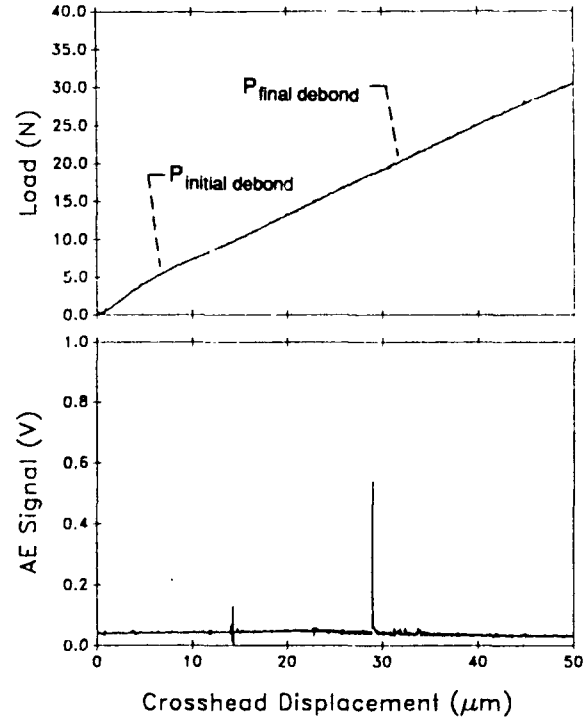
Figure 4.—Fiber push-out load/displacement and AE/displacement plots for as-fabricated SiC/RBSN composite specimens of different thicknesses.
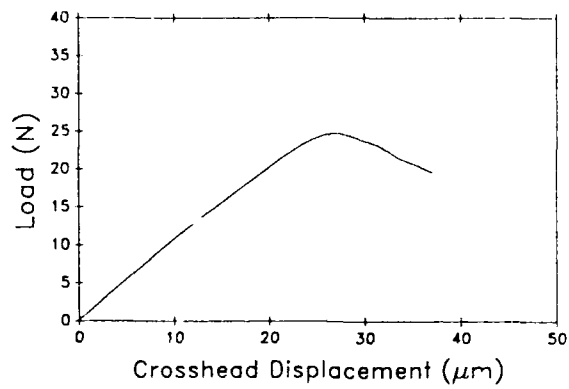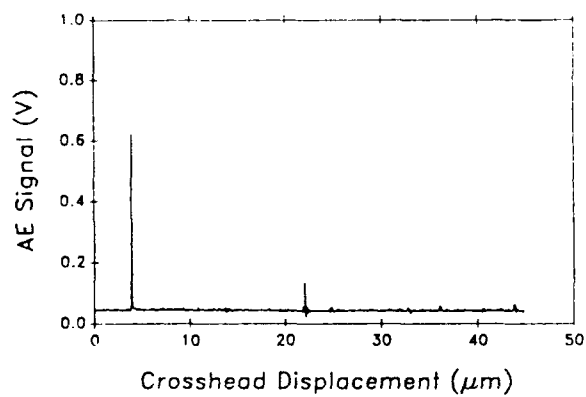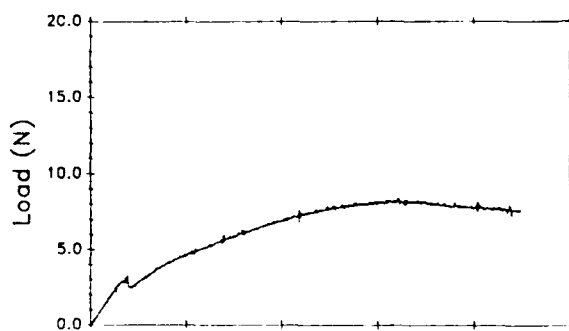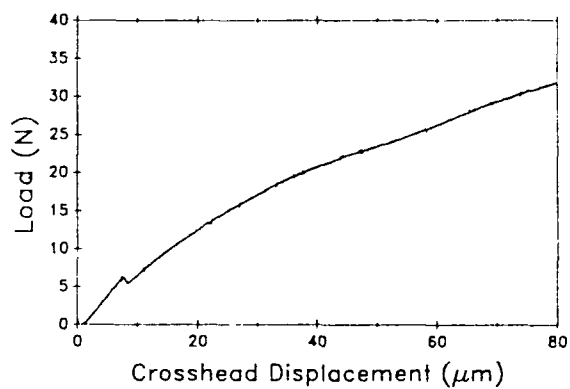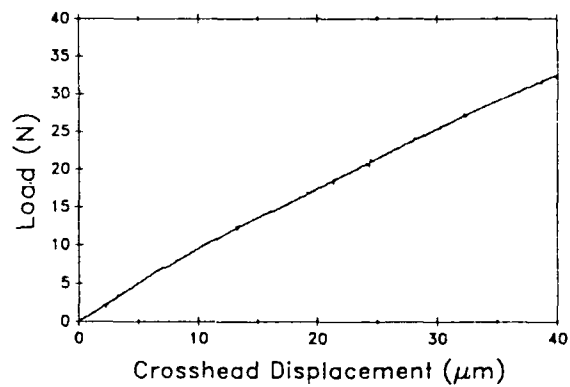
(a) Thickness = 1.93 mm.

(b) Thickness = 3.73 mm.

Figure 5.—Fiber push-out load/displacement plots
for SiC/RBSN composite HIPed at high
temperature. No AE was observed.

11

Figure 6.—Fiber push-out load/displacement plots for SiC/RBSN composite HIPed at low temperature. AE was only observed for 0.51 mm thick sample.
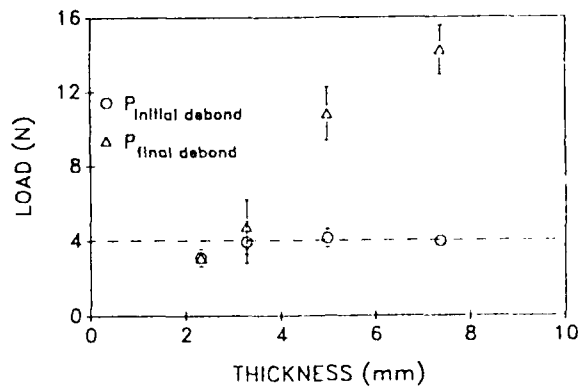
(a) Initial and final debond loads, $P_{initial\ debond}$ and $P_{final\ debond}$.
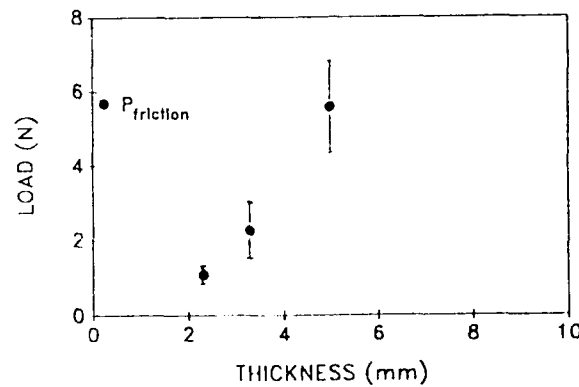
(b) Frictional sliding loads, $P_{friction}$.

Figure 7.—Push-out loads as a function of sample thickness for as-fabricated SiC/RBSN composite.
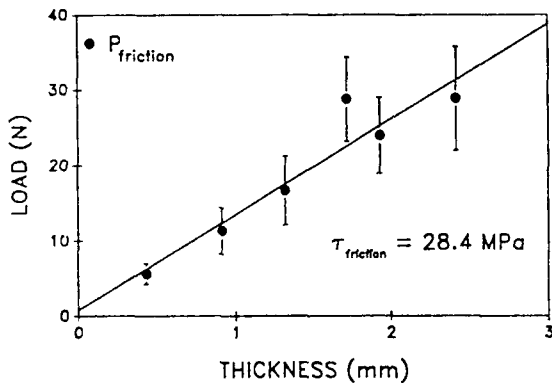
Figure 8.—Frictional sliding push-out loads, $P_{friction}$, as a function of sample thickness for SiC/RBSN composite HIPed at high temperature. Solid line is a least squares fit of data to Equation 1.
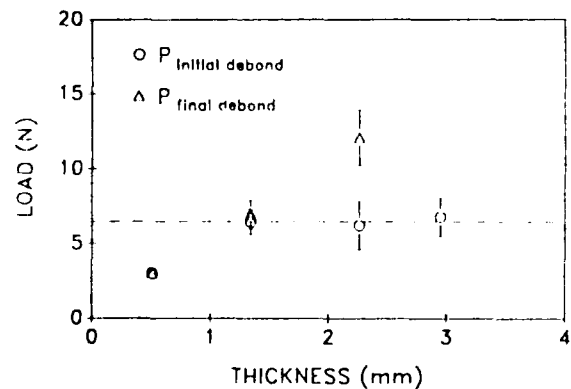
Figure 9.—Initial and final debond push-out loads, $P_{initial\ debond}$ and $P_{final\ debond}$, as a function of sample thickness for SiC/RBSN composite HIPed at low temperature.
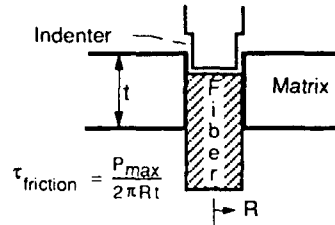
(a) Schematic of punch-out test.

$$\tau_{friction} = \frac{P_{max}}{2\pi R t}$$

$$u - \frac{P}{K_{machine}}$$

$$u = \frac{P^2}{4\pi^2 R^3 \tau E_f} + \frac{P}{K_{machine}}$$
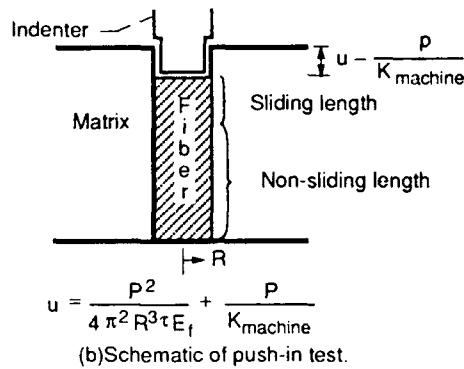
(b) Schematic of push-in test.

- - - Linear machine response
—— 2nd-order polynomial fit

From curvature
$\tau = 27.9$ MPa

From peak load
$\tau = 28.9$ MPa

1.93 mm SiC/Si$_3$N$_4$- HIPed
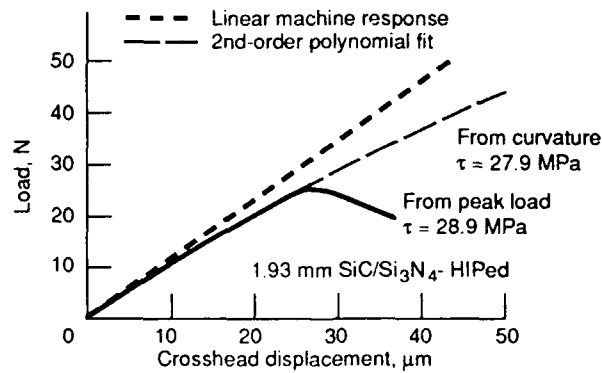
(c) Fiber push-out load/displacement curve.

Figure 10.—Push-out and push-in for 1.93 mm
thick SiC/RBSN HIPed at high temperature
showing fit of initial curvature to Equation 2.

14
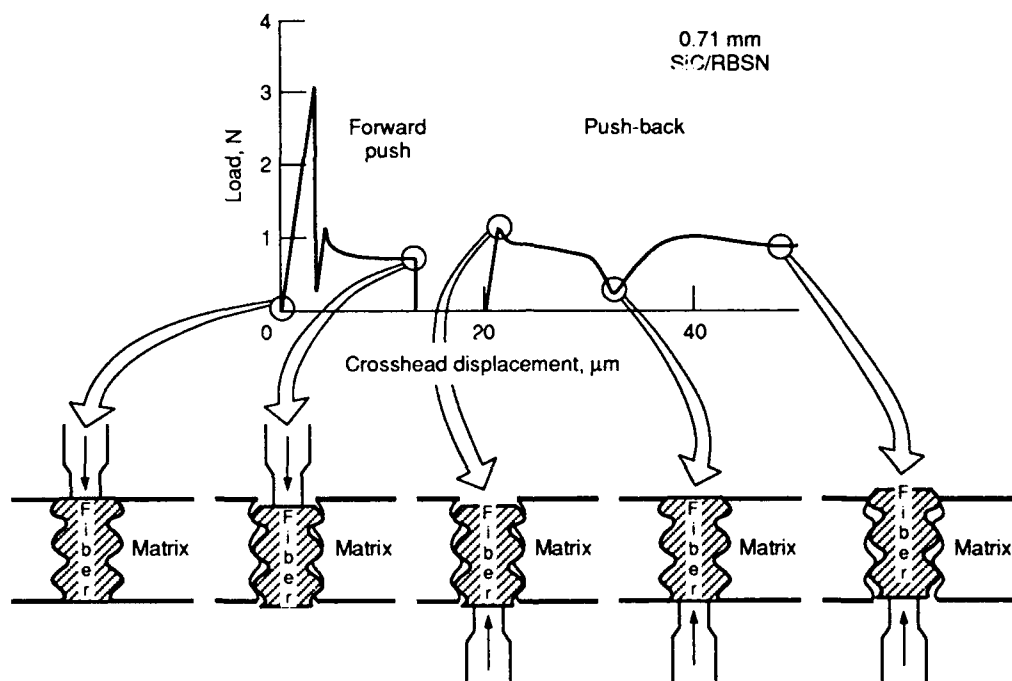
Figure 11.—Schematic diagram showing position of fiber relative to points on the fiber push-out and push-back load/displacement curves.
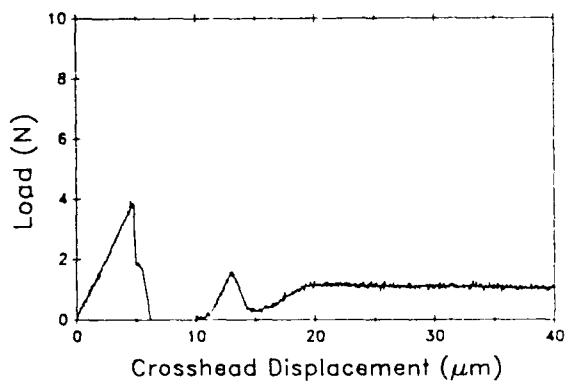
(a) 2.31 mm thick as-fabricated SiC/RBSN composite.
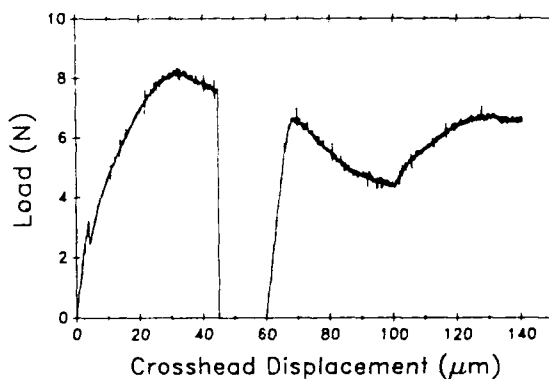
(a) 2.31 mr · ·ck as-fabricated SiC/RBSN composite.

(b) 0.51 mm thick SiC/RBSN HIPed at low temperature.
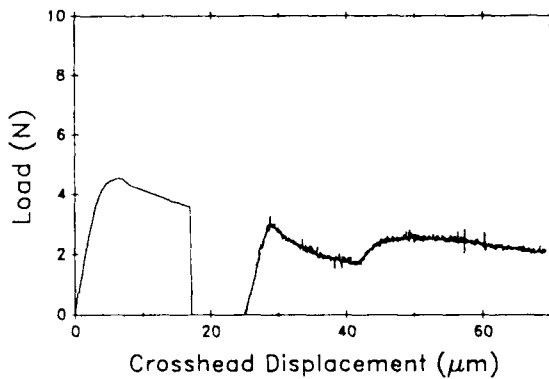
(b) 0.51 mm thick SiC/RBSN HIPed at low temperature.

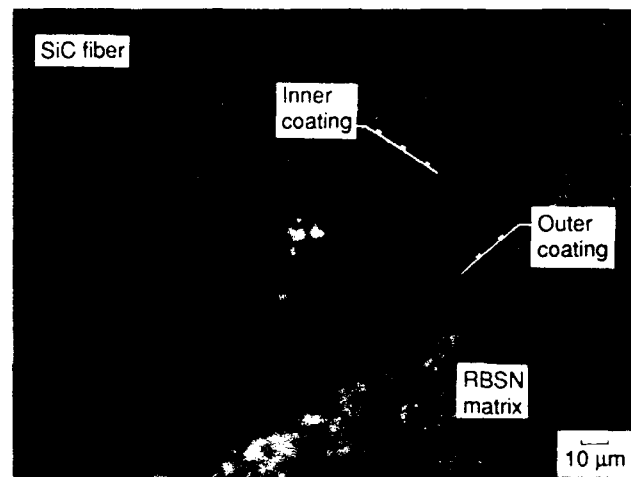(c) 0.43 mm thick SiC/RBSN HIPed at high temperature.

(c) 0.43 mm thick SiC/RBSN HIPed at high temperature.

Figure 12.—Fiber push-out and push-back load/ displacement curves with short initial displacements.
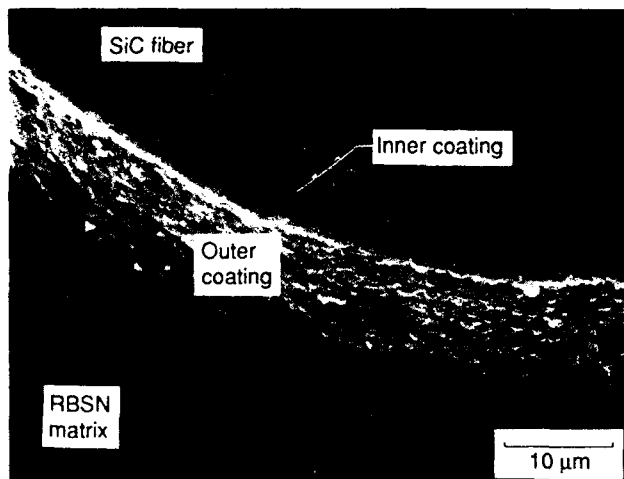
Figure 13.—Fiber push-out and push-back load/ displacement curves with long initial displacements.
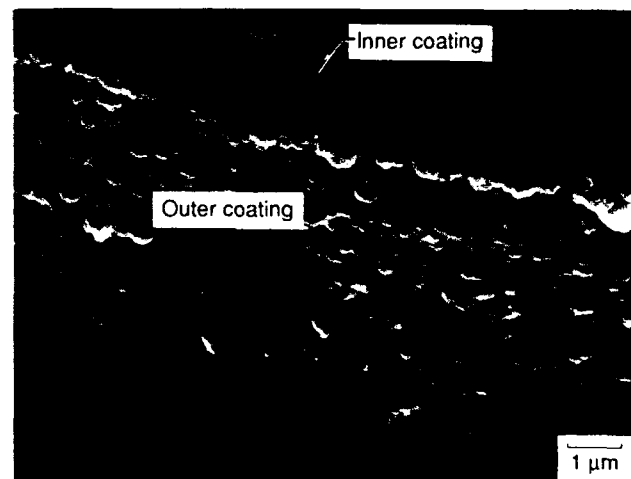
16
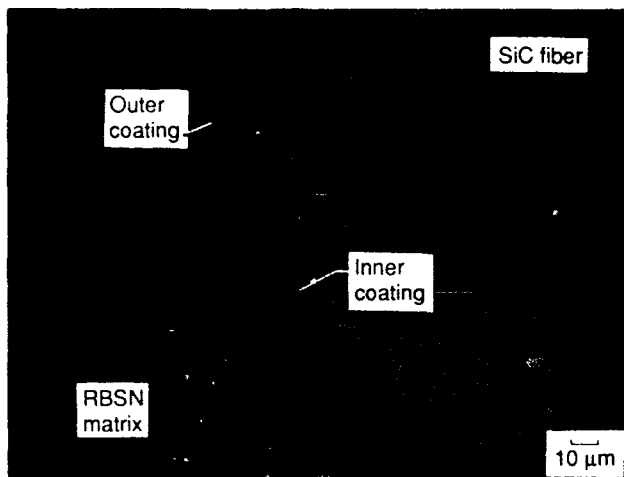
(a) Undisplaced fiber in as-fabricated SiC/RBSN.

(b) Pushed-out fiber in as-fabricated SiC/RBSN.

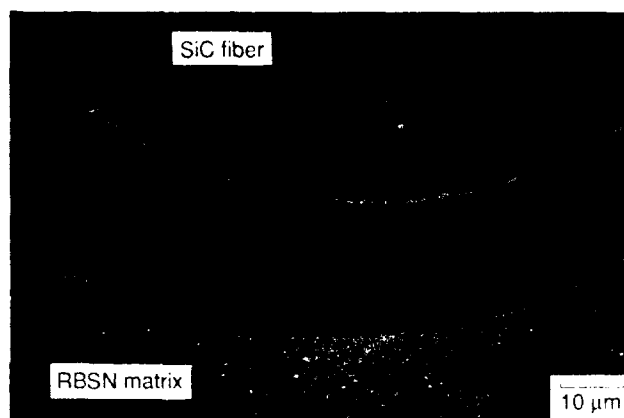(c) Pushed-out fiber in SiC/RBSN HIPed at high temperature.

(d) Same as (c) but at higher magnification showing asperities on surface of exposed coating.

Figure 14.—SEM micrographs of pushed-out fibers.

(e) Low magnification of a fiber pushed-out of SiC/RBSN HIPed at low temperature.

(f) Higher magnification of a fiber pushed-out of SiC/RBSN HIPed at low temperature.

Figure 14.—Concluded.

NASA

National Aeronautics and Space Administration

Report Documentation Page

1. Report No. NASA TM -103739 AVSCOM TR 91 - C-006	2. Government Accession No.	3. Recipient's Catalog No.

4. Title and Subtitle	5. Report Date
Investigation of Interfacial Shear Strength in SiC/Si_3N_4 Composites	
	6. Performing Organization Code

7. Author(s)	8. Performing Organization Report No.
J.I. Eldridge, R.T. Bhatt, and J.D. Kiser	E -5979
	10. Work Unit No.

9. Performing Organization Name and Address	510-01-0A
NASA Lewis Research Center Cleveland, Ohio 44135 - 3191 and Propulsion Directorate U.S. Army Aviation Systems Command Cleveland, Ohio 44135 - 3191	1L161102AH45
	11. Contract or Grant No.

12. Sponsoring Agency Name and Address	13. Type of Report and Period Covered
National Aeronautics and Space Administration Washington, D.C. 20546 - 0001 and U.S. Army Aviation Systems Command St. Louis, Mo. 63120 - 1798	Technical Memorandum
	14. Sponsoring Agency Code

16. Abstract

A fiber push-out technique was used to determine fiber/matrix interfacial shear strength (ISS) for silicon carbide fiber reinforced reaction-bonded silicon nitride (SiC/RBSN) composites in the as-fabricated condition and after consolidation by hot isostatic pressing (HIPing). In situ video microscopy and acoustic emission detection greatly aided the interpretation of push-out load/displacement curves. The as-fabricated and HIPed SiC/RBSN composites showed very different fiber push-out behavior as reflected by differently shaped load/displacement curves. The push-out data revealed the presence of definite, but weak, fiber/matrix bonding in both the as-fabricated composite and a composite HIPed at low temperature and showed the absence of fiber/matrix bonding in a composite HIPed at high temperature. The HIPed composites exhibited significantly higher frictional interfacial shear stresses as well as evidence of interfacial wear during fiber sliding. Finally, fiber push-out testing of different thickness samples revealed two regimes of fiber/matrix debonding behavior. For thinner samples, a single complete debonding event occurs; whereas, for thicker samples, a debond initiation of a critical length occurs and is followed by stable debond propagation with increasing applied load.

17. Key Words (Suggested by Author(s))	18. Distribution Statement
Ceramic matrix composites Solid-solid interfaces Hot isostatic pressing Shear strength	Unclassified - Unlimited Subject Categories 24 and 27

19. Security Classif. (of the report)	20. Security Classif (of this page)	21. No. of pages	22 Price*
Unclassified	Unclassified	20	A03

National Aeronautics and
Space Administration

Lewis Research Center
Cleveland, Ohio 44135

FOURTH CLASS MAIL

ADDRESS CORRECTION REQUESTED

NASA